Progress In Electromagnetics Research, Vol. 141, 659–670, 2013

COHERENT ANTI-STOKES RAMAN SCATTERING MICROSCOPY BY DISPERSIVE WAVE GENERATIONS IN A POLARIZATION MAINTAINING PHOTONIC CRYSTAL FIBER

Jinhui Yuan[1, 2], Guiyao Zhou[1, 3, *], Hongzhan Liu[1], Changming Xia[1], Xinzhu Sang[2], Qiang Wu[2, 4], Chongxiu Yu[2], Kuiru Wang[2], Binbin Yan[2], Ying Han[3], Gerald Farrell[2, 4], and Lantian Hou[3]

[1]Laboratory of Nanophotonic Functional Materials and Devices, South China Normal University, Guangzhou 510006, China

[2]State Key Laboratory of Information Photonics and Optical Communications, Beijing University of Posts and Telecommunications, P. O. Box163 (BUPT), Beijing 100876, China

[3]Institute of Infrared Optical Fibers and Sensors, Physics Department, Yanshan University, Qinhuangdao 066004, China

[4]Photonics Research Center, School of Electronic and Communications Engineering, Dublin Institute of Technology, Kevin Street, Dublin 8, Ireland

Abstract—The polarization maintaining photonic crystal fiber (PM-PCF) with two zero dispersion wavelengths is designed and fabricated by the improved stack-and-draw technology in our laboratory. The broadband blue-shifted and red-shifted dispersive waves (DWs) are efficiently generated from soliton self-frequency shift (SSFS) along the slow axis of PM-PCF. By optimizing the pump parameters and the fiber length, the polarized DWs centered in the normal dispersion region can be used as the pump and Stokes pulses for the high resolution coherent anti-Stokes Raman scattering (CARS) microscopy. Moreover, it is demonstrated that the widely tunable relevant CARS wavelengths can be obtained by adjusting the pump wavelength. The CARS microscopy based on DWs can find important applications in detecting the biological and chemical samples with the $C = N$, S-H, C-H, and O-H stretch vibration resonances of 2100 to 2400 cm^{-1}, 2500 to 2650 cm^{-1}, 2700 to 3000 cm^{-1}, and 3000 to 3750 cm^{-1}.

Received 3 July 2013, Accepted 30 July 2013, Scheduled 5 August 2013

* Corresponding author: Guiyao Zhou (zguiyao@163.com).

1. INTRODUCTION

Coherent anti-Stokes Raman scattering (CARS) is a nonlinear scattering process arising from the third-order nonlinear susceptibility $\chi^{(3)}$, where the pump beam at ω_P and Stokes beam at ω_S overlap temporally and spatially in the samples and the anti-Stokes beam at $\omega_{AS} = 2\omega_P - \omega_S$ is generated. One of the successful applications is the CARS microscopy [1–6], which has proved to be a powerful tool for the chemical imaging of biological and material systems. Because of the coherence and nonlinear dependence on the excitation intensity of Stokes beams, the CARS microscopy as a high resolution nonlinear imaging technique has a fast data acquisition time and 3-dimensional sectioning capability. However, the conventional CARS setups aren't widely adopted since the systems are complex and the light sources for generating the pump and Stokes beams are very expensive.

Photonic crystal fibers (PCFs) [7–12] have attracted great attention due to the high nonlinearity and the tailored dispersion profile. By designing the structures of PCFs, it is possible to tailor the output spectral distribution for concentrating the power at the desired spectral ranges relevant for the CARS microscopy [13–17]. Over the last few years, the CARS microscopy with PCFs has been developed to simplify the system and reduce the costs. Up to now, some frequency conversion techniques based on the supercontinuum [18–23] or the non-supercontinuum [24–30] have been used to generate the pump and Stokes beams. The selective spectral filtering of supercontinuum can obtain the desired wavelengths, but the temporal width can be elongated as well as the decreased spectral energy, and the noise amplification is remarkable due to the complex nonlinear optical process. Several nonlinear effects, such as stimulated Raman scattering (SRS), four-wave mixing (FWM), soliton fission, and dispersive waves (DWs) have been demonstrated to generate the narrowband spectral components for the pump and Stokes beams through adjusting the location of the excitation wavelength relative to the zero-dispersion wavelength of PCFs. However, the conversion efficiency from the pump to the Stokes beam is low, along with the narrow bandwidth of the Stokes beam. In addition, the polarization state of Stokes beam interacting with the samples can not be well controlled, leading to the severe interference of the non-resonant background with $\chi^{(3)}$ and the reduction of resolution for the CARS microscopy.

In this paper, a polarization maintaining PCF (PM-PCF) with two zero dispersion wavelengths is designed and fabricated in our laboratory. The broadband blue-shifted and red-shifted DWs are efficiently generated from soliton self-frequency shift (SSFS) along

the slow axis of PM-PCF. Two DW peaks centered in the normal dispersion region can be used as the pump and Stokes pulses for the high resolution CARS microscopy.

2. PCF PROPERTIES AND EXPERIMENT

The PM-PCF is designed and fabricated by the improved stack-and-draw technology. The calculated group velocity dispersion curves for the fundamental mode of PM-PCF with two zero dispersion wavelengths along the fast axis of 769 nm and 929 nm and the slow axis of 794 nm and 887 nm are presented in Fig. 1. The cross-section of PM-PCF with the average relative hole size of 0.9 and the nonlinear coefficient of 0.145 to 0.165 $W^{-1}m^{-1}$ is shown in the inset, where an elliptically deformed core gives rise to form the birefringence and the diameters of slow and fast axis are 2.25 μm and 1.9 μm with the ratio of 1.18.

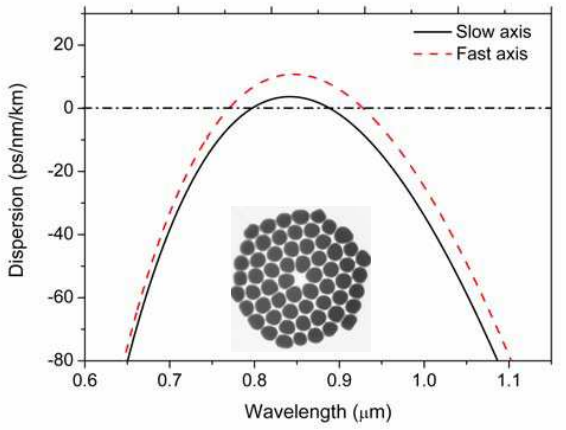

Figure 1. Group velocity dispersion curves calculated for the fundamental mode of PM-PCF along the slow and fast axis, the inset showing the cross-section of PM-PCF used in the experiment.

The short pulses generated from a mode-locked (Kerr Lens Modelocking, KLM) Ti: sapphire ultrafast laser with the 120 fs pulse width and the central wavelength of 800 nm at a repetition rate of 76 MHz are coupled into a span of PM-PCF, and the coupling efficiency can be up to 65%. An isolator is inserted to prevent the back-reflection light into the laser cavity, and a variable attenuator is used to adjust the input power. The stretch of pulse is compensated by a prism

compressor, and the polarization state of pump light is controlled by a half-wave plate. By the offset pumping technique, the fundamental mode can be selectively excited. The propagation loss is measured to be 2.1 dB/m at 800 nm by the cut-back method. The output spectra from the PM-PCF are monitored by two optical spectrum analyzers (OSA, Avaspec-256 and Avaspec-NIR-256) with the measurement scopes of 200 to 1100 nm and 900 to 2500 nm and the resolutions of 0.025 nm and 15 nm.

3. RESULTS AND DISCUSSION

Taking into account the Kerr and Raman contributions to the nonlinearity, the self-steepening (SS), the loss of pump field, the influence of the wavelength-dependent effective mode area, and the fourth-order group velocity dispersion, the simulation results using the nonlinear Schrödinger equation (NLSE) [31, 32] can exactly predict the evolution of femtossecond pulses inside a span of PM-PCF with a length of 55 cm for the pump wavelength of 785 nm and the average power of 300 mW. As presented in Figs. 2(a) and (b), the simulation results agree well with the experimental ones.

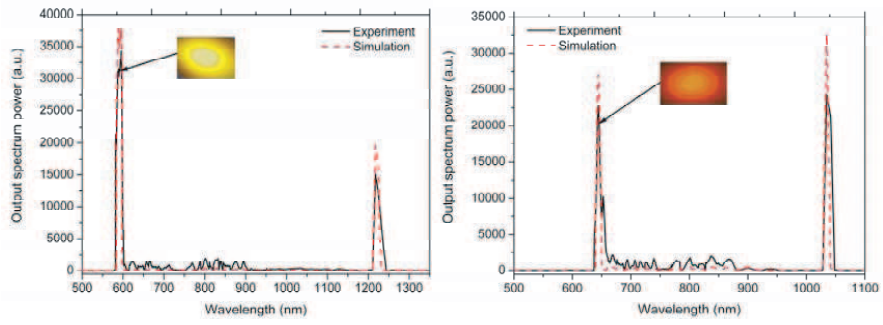

Figure 2. The output spectra for the pump wavelength of 785 nm and the average power of 300 mW with the PM-PCF length of 55 cm along, (a) the fast axis, and (b) the slow axis. The insets show the observed output far fields of DW1, the yellow light and the red-orange light.

In Fig. 2(a), when the pump pulse with the wavelength of 785 nm and the average power of 300 mW polarize along the fast axis, the central wavelength of pump pulse lies on the positive slope of the PM-PCF dispersion profile in the anomalous dispersion region, and the

soliton is formed due to the interplay between the negative dispersion and the self-phase modulation (SPM). The soliton continuously shifts toward the longer wavelength as it propagates through the PM-PCF owing to the intrapulse Raman scattering (IRS). At the same time, the resonant dispersive wave 1 (DW1) is generated at the shorter wavelength of 590 nm due to the perturbation induced by the higher-order dispersions and the resonance matching condition, which is predominantly the blue-shifted branch. As the central wavelength of soliton is shifted to the negative slope of the PM-PCF dispersion profile, the dispersive wave 2 (DW2) as the red-shifted branch is generated at the longer wavelength of 1220 nm. The Raman shifts of DW1 and DW2 are 4210 cm^{-1} and 4542 cm^{-1}. In Fig. 2(b), when the same pump pulse polarizes along the slow axis, the central wavelength of pump pulse lies within the normal dispersion region closing to the first zero dispersion wavelength, the input spectrum of pump pulse is broadened into the anomalous dispersion region by SPM, and the red-shifted soliton generates the DW1 and DW2 located at two peaks of 645 nm and 1035 nm in the normal dispersion region, corresponding to the Raman shifts of 2765 cm^{-1} and 3077 cm^{-1}. The red-shift ability of soliton will be cancelled by the spectral recoil from the amplified DW2, which acts on the soliton and compensates for the Raman frequency shift when the soliton approaches the second zero dispersion wavelength. As shown in the insets of Figs. 2(a) and (b), the observed output far field intensities of DW1 reach the maximum at the center of the fiber core and monotonically decrease with the distance from the center of the core, showing the spatial distribution characteristic of fundamental mode. By comparing Figs. 2(a) and (b), the polarization can be optimized along the slow axis, and the generated DW1 and DW2 accompanied by almost total depletion inside the anomalous dispersion region can be used as the pump and Stokes beams for the high resolution CARS imaging of samples with the C-H and O-H stretch vibration resonances of 2700 to 3000 cm^{-1} and 3000 to 3750 cm^{-1}.

When the pump pulses with the wavelength of 800 nm and the average power P_{av} of 100 to 300 mW polarize along the slow axis, the low anomalous dispersion between two zero dispersion wavelengths can initiate the SPM for the spectral broadening. The frequency of soliton gets shifted in the spectral direction opposite to that of the DWs to conserve the overall energy of the photons. The DW1 and DW2 are effectively generated in the wavelength ranges of 657 to 637 nm and 1035 to 1023 nm as the pump and soliton inside the anomalous dispersion region are greatly depleted, and the corresponding Raman shifts are from 2721 to 3199 cm^{-1} and 2838 to 2725 cm^{-1}, as shown in

Figs. 3(a), (b), and (c).

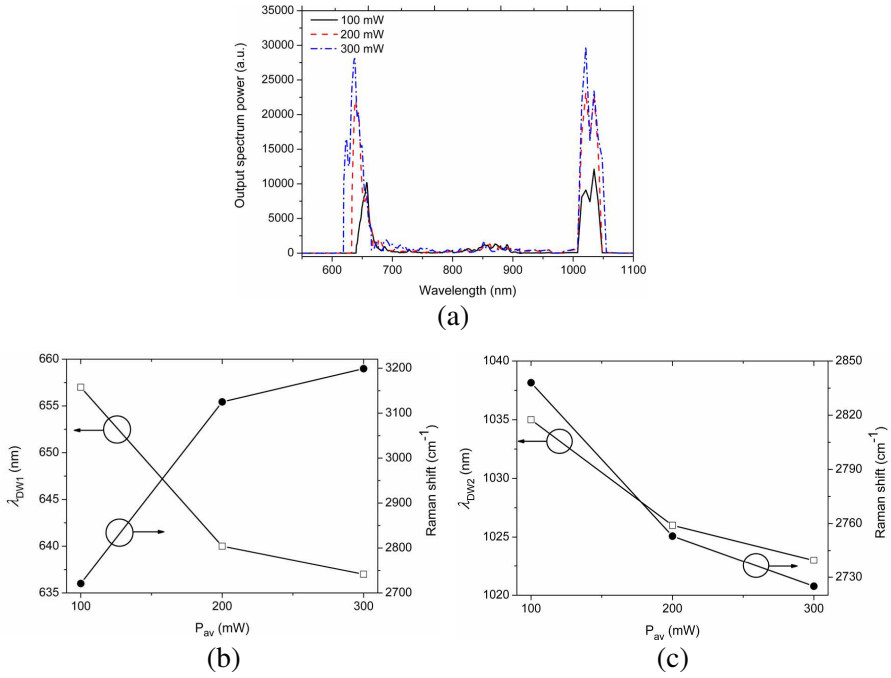

Figure 3. (a) The output spectra for the pump wavelength of 800 nm and P_{av} of 100 to 300 mW with the PCF length of 55 cm along the slow axis, (b) the central wavelength λ_{DW1} and Raman shift of DW1 as functions of P_{av}, and (c) the central wavelength λ_{DW2} and Raman shift of DW2 as functions of P_{av}.

As shown in Figs. 4(a), (b), and (c), when the pump operates at the wavelength λ_P of 800 nm and P_{av} of 300 mW along the slow axis, two DW peaks are centered in the wavelength ranges of 656 to 632 nm and 1050 to 1017 nm as the PM-PCF length increases from 45 to 65 cm, and the corresponding Raman shifts of 2744 to 3323 cm^{-1} and 2976 to 2667 cm^{-1} are relevant for the CARS regions for the samples with the C-H and O-H stretch vibrations. Figs. 4(d) and (e) show the relationships between the conversion efficiency η_{DW1} and bandwidth B_{DW1} of DW1 and the PM-PCF length L, and the relationships between the conversion efficiency η_{DW2} and bandwidth B_{DW2} of DW2 and L. η_{DW1} and η_{DW2} can be defined as the ratio of the output power P_{DW1} and P_{DW2} of DW1 and DW2 and the incident power P_0 of pump. For the coupling efficiency of 65%, P_{DW1} and P_{DW2} are measured to be 21.45 mW, 33.15 mW, and 30.07 mW; 25.35 mW,

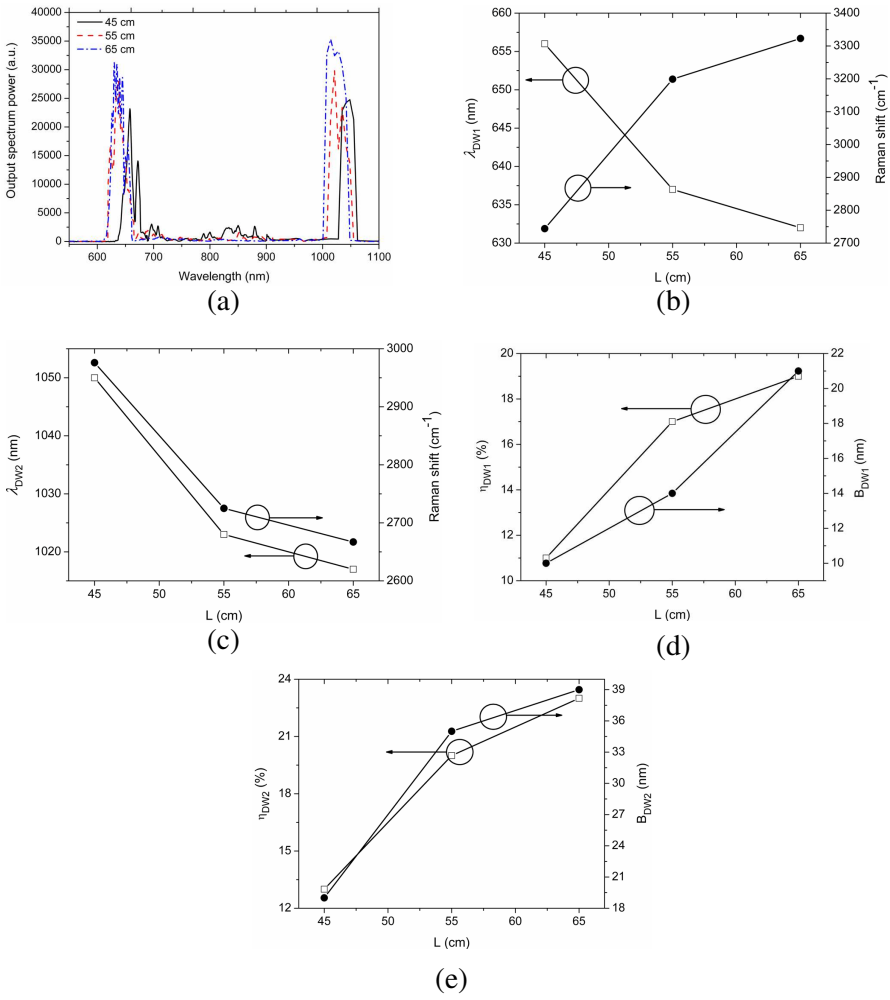

Figure 4. (a) The output spectra for λ_P of 800 nm and P_{av} of 300 mW with L of 45 to 65 cm along the slow axis, (b) λ_{DW1} and Raman shift of DW1 as functions of L, (c) λ_{DW2} and Raman shift of DW2 as functions of L, (d) η_{DW1} and B_{DW1} of DW1 as functions of L, and (e) η_{DW2} and B_{DW2} of DW2 as functions of L.

39 mW, and 44.85 mW, and the corresponding η_{DW1} and η_{DW2} can be up to 11%, 17%, and 19%; 13%, 20%, and 23%. B_{DW1} and B_{DW2} are broadened to be 10 nm, 14 nm, and 21 nm; 19 nm, 35 nm, and 39 nm.

As demonstrated in above results, the PM-PCF can be determined to be a suitable candidate as a CARS source based on its spectral

properties, the output spectra are concentrated around two relevant CARS wavelengths in the blue-shifted and red-shifted DWs in the normal dispersion region. In Figs. 5(a) and (b), when the pump pulses with P_{av} of 300 mW and λ_P of 790 to 820 nm are propagated along the slow axis inside the PCF with a length of 65 cm, the central wavelengths of DW1 and DW2 change from 639 to 623 nm and 1026 to 1006 nm, which correspond to the Raman shifts of 2991 to 3856 cm^{-1} and 2912 to 2255 cm^{-1}. Thus, the widely tunable relevant CARS wavelengths are obtained, which can find important applications in detecting the biological and chemical samples with the $C = N$, S-H, C-H, and O-H stretch vibration resonances of 2100 to 2400 cm^{-1}, 2500 to 2650 cm^{-1}, 2700 to 3000 cm^{-1}, and 3000 to 3750 cm^{-1}.

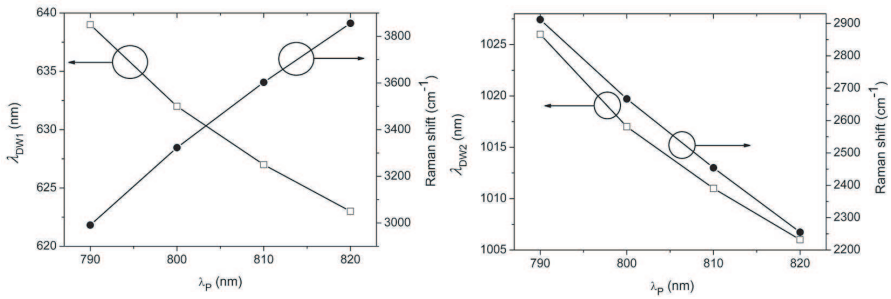

Figure 5. For P_{av} of 300 mW and λ_P of 790 to 820 nm in a PM-PCF with L of 65 cm along the slow axis, (a) λ_{DW1} and Raman shift of DW1 as functions of λ_P, and (b) λ_{DW2} and Raman shift of DW2 as functions of λ_P.

4. CONCLUSION

In summary, the broadband blue-shifted and red-shifted DWs based on SSFS are efficiently generated in a PM-PCF with two zero dispersion wavelengths designed and fabricated in our laboratory. The high conversion efficiency, broad bandwidth, and widely tunable DWs centered in two relevant CARS regions can constitute an important progress in the development of a simple and compact CARS microscopy with the high resolution for detecting the biological and chemical samples with the $C = N$, S-H, C-H, and O-H stretch vibration resonances of 2100 to 2400 cm^{-1}, 2500 to 2650 cm^{-1}, 2700 to 3000 cm^{-1}, and 3000 to 3750 cm^{-1}.

ACKNOWLEDGMENT

This work is partly supported by the National Basic Research Program (2010CB327604, 2010CB327605, and 2010CB328300), the National High-Technology Research and Development Program of China (2013AA031501), the key grant of Ministry of Education (109015), the Program for New Century Excellent Talents in University (NECT-11-0596) and Beijing Nova program (2011066), the Specialized Research Fund for the Doctoral Program of Higher Education (20120005120021), the Fundamental Research Funds for the Central Universities (2013RC1202), the China Postdoctoral Science Foundation (2012M511826), and the Postdoctoral Science Foundation of Guangdong Province (244331).

REFERENCES

1. Duncan, M. D., J. Reintjes, and T. J. Manuccia, "Scanning coherent anti-Stokes Raman microscope," *Opt. Lett.*, Vol. 7, 350–352, 1982.
2. Cheng, J. X., L. D. Book, and X. S. Xie, "Polarization coherent anti-Stokes Raman scattering microscopy," *Opt. Lett.*, Vol. 26, 1341–1343, 2001.
3. Evans, C. L., E. O. Potma, and X. S. Xie, "Coherent anti-Stokes Raman scattering spectral interferometry: Determination of the real and imaginary components of nonlinear susceptibility $\chi(3)$ for vibrational microscopy," *Opt. Lett.*, Vol. 29, 2923–2925, 2004.
4. Kee, T. W. and M. T. Cicerone, "Simple approach to one-laser, broadband coherent anti-Stokes Raman scattering microscopy," *Opt. Lett.*, Vol. 29, 2701–2703, 2004.
5. Lefrancois, S., D. Fu, G. R. Holtom, L. Kong, W. J. Wadsworth, P. Schneider, R. Herda, A. Zach, X. S. Xie, and F. W. Wise, "Fiber four-wave mixing source for coherent anti-Stokes Raman scattering microscopy," *Opt. Lett.*, Vol. 37, 1652–1654, 2012.
6. Baumgartl, M., M. Chemnitz, C. Jauregui, T. Meyer, B. Dietzek, J. Popp, J. Limpert, and A. Tünnermann, "All-fiber laser source for CARS microscopy based on fiber optical parametric frequency conversion," *Opt. Express*, Vol. 20, 4484–4493, 2012.
7. Russell, P. St. J., "Photonic crystal fibers," *Science*, Vol. 299, 358–362, 2003.
8. Knight, J. C., "Photonic crystal fibres," *Nature*, Vol. 424, 847–851, 2003.

9. Russell, P. St. J., "Photonic crystal fibers," *J. Lightw. Technol.*, Vol. 24, 4729–4749, 2006.
10. Dudley, J. M. and J. R. Taylor, "Ten years of nonlinear optics in photonic crystal fibre," *Nature Photon.*, Vol. 3, 85–90, 2009.
11. Guenneau, S., A. Nicolet, F. Zolla, and S. Lasquellec, "Numerical and theoretical study of photonic crystal fibers," *Progress In Electromagnetics Research*, Vol. 41, 271–305, 2003.
12. Chen, D., M.-L. V. Tse, and H. Y. Tam, "Optical properties of photonic crystal fibers with a fiber core of arrays of subwavelength circular air holes: Birefringence and dispersion," *Progress In Electromagnetics Research*, Vol. 105, 193–212, 2010.
13. Paulsen, H. N., K. M. Hilligsøe, J. Thøgersen, S. R. Keiding, and J. J. Larsen, "Coherent anti-Stokes Raman scattering microscopy with a photonic crystal fiber based light source," *Opt. Lett.*, Vol. 28, 1123–1125, 2003.
14. Andresen, E. R. and H. N. Paulsen, "Broadband multiplex coherent anti-Stokes Raman scattering microscopy employing photonic-crystal fibers," *J. Opt. Soc. Am. B*, Vol. 22, 1934–1938, 2005.
15. Murugkar, S., C. Brideau, A. Ridsdale, M. Naji, P. K. Stys, and H. Anis, "Coherent anti-Stokes Raman scattering microscopy using photonic crystal fiber with two closely lying zero dispersion wavelengths," *Opt. Express*, Vol. 15, 14028–14037, 2007.
16. Savvin, A. D., A. A. Lanin, A. A. Voronin, A. B. Fedotov, and A. M. Zheltikov, "Coherent anti-Stokes Raman metrology of phonons powered by photonic-crystal fibers," *Opt. Lett.*, Vol. 35, 919–921, 2010.
17. Klarskov, P., A. Isomäki, K. P. Hansen, and P. E. Andersen, "Supercontinuum generation for coherent anti-Stokes Raman scattering microscopy with photonic crystal fibers," *Opt. Express*, Vol. 19, 26672–26683, 2011.
18. Coen, S., A. H. L. Chau, R. Leonhardt, J. D. Harvey, J. C. Knight, W. J. Wadsworth, and P. St. J. Russell, "White-light supercontinuum generation with 60-ps pump pulses in a photonic crystal fiber," *Opt. Lett.*, Vol. 26, 1356–1358, 2001.
19. Wadsworth, W. J., A. Ortigosa-Blanch, J. C. Knight, T. A. Birks, T. P. M. Man, and P. St. J. Russell, "Supercontinuum generation in photonic crystal fibers and optical fiber tapers: A novel light source," *J. Opt. Soc. Am. B*, Vol. 19, 2148–2155, 2002.
20. Dudley, J. M., L. Provino, N. Grossard, H. Maillotte, R. S. Windeler, B. J. Eggleton, and S. Coen, "Supercontinuum

generation in air-silica microstructured fibers with nanosecond and femtosecond pulse pumping," *J. Opt. Soc. Am. B*, Vol. 19, 765–771, 2002.

21. Saitoh, K. and M. Koshiba, "Highly nonlinear dispersion-flattened photonic crystal fibers for supercontinuum generation in a telecommunication window," *Opt. Express*, Vol. 12, 2027–2032, 2004.
22. Dudley, J. M., G. Genty, and S. Coen, "Supercontinuum generation in photonic crystal fiber," *Rev. Mod. Phys.*, Vol. 78, 1135–1184, 2005.
23. Mitrokhin, V. P., A. A. Ivanov, A. B. Fedotov, M. V. Alfimov, K. V. Dukel'skii, A. V. Khokhlov, V. S. Shevandin, Y. N. Kondrat'ev, A. A. Podshivalov, and A. M. Zheltikov, "Spectral transformation ofmegawatt femtosecond optical pulses in large-mode-area high-index-step photonic-crystal fibers," *Laser Phys. Lett.*, Vol. 4, 529–533, 2007.
24. Abedin, K. S., J. T. Gopinath, E. P. Ippen, C. E. Kerbage, R. S. Windeler, and B. J. Eggleton, "Highly nondegenerate femtosecond four-wave mixing in tapered microstructure fiber," *Appl. Phys. Lett.*, Vol. 81, 1384–1386, 2002.
25. Yang, T. T., C. Shu, and C. Lin, "Depolarization technique for wavelength conversion using four-wave mixing in a dispersion-flattened photonic crystal fiber," *Opt. Express*, Vol. 13, 5409–415, 2005.
26. Hu, M. L., C. Y. Wang, Y. J. Song, Y. F. Li, and L. Chai, "Mode-selective mapping and control of vectorial nonlinear-optical processes in multimode photonic-crystal fibers," *Opt. Express*, Vol. 14, 1189–1198, 2006.
27. Asimakis, S., P. Petropoulos, F. Poletti, J. Y. Y. Leong, R. C. Moore, K. E. Frampton, X. Feng, W. H. Loh, and D. J. Richardson, "Towards efficient and broadband four-wave-mixing using short-length dispersion tailored lead silicate Holey fibers," *Opt. Express*, Vol. 15, 596–601, 2007.
28. Sloanes, T., K. McEwan, B. Lowans, and L. Michaille, "Optimisation of high average power optical parametric generation using a photonic crystal fiber," *Opt. Express*, Vol. 16, 19724–19733, 2008.
29. Yuan, J. H., X. Z. Sang, C. X. Yu, Y. Han, G. Y. Zhou, S. G. Li, and L. T. Hou, "Highly efficient and broadband Cherenkov radiation at the visible wavelength in the fundamental mode of photonic crystal fiber," *IEEE Photon. Technol. Lett.*, Vol. 23, 786–788, 2011.

30. Yuan, J. H., X. Z. Sang, Q. Wu, C. X. Yu, X. W. Shen, K. R. Wang, B. B. Yan, Y. Han, G. Y. Zhou, Y. Semenova, G. Farrell, and L. T. Hou, "Efficient red-shifted dispersive wave in a photonic crystal fiber for widely tunable mid-infrared wavelength generation," *Laser Phys. Lett.*, Vol. 10, 045405-1-5, 2013.
31. Peng, J. H., A. V. Sokolov, F. Benabid, F. Biancalana, P. S. Light, F. Couny, and P. J. Roberts, "Widely tunable femtosecond solitonic radiation in photonic crystal fiber cladding," *Phys. Rev. A*, Vol. 81, 031803(R)-1–031803(R)-4, 2010.
32. Serebryannikov, E. E., A. M. Zheltikov, S. Köhler, N. Ishii, C. Y. Teisset, T. Fuji, F. Krausz, and A. Baltuška, "Diffraction-arrested soliton self-frequency shift of few-cycle laser pulses in a photonic-crystal fiber," *Phys. Rev. E*, Vol. 73, 066617-1–066617-4, 2006.